HEAT TRANSFER PROFILES OF AN IMPINGING ATOMIZING WATER-AIR MIST JET

Cian Quinn* , **Tim Persoons*** and **Darina B Murray***

* Dept. Mechanical & Manufacturing Engineering, Trinity College Dublin, Ireland
E-mail : ciquinn@tcd.ie

ABSTRACT

This paper presents experimental work on the heat transfer characteristics of an impinging water-air atomizing mist jet. Time averaged local heat transfer profiles for varying water to air flow rate ratios, Reynolds numbers and nozzle to plate spacings are presented. It is found that increasing the amount of water in the mist jet does not necessarily increase the stagnation zone heat transfer, but can lead to an increased spatial average of the heat transfer coefficient. Very low mist loading fractions - below 0.01 - were found to offer heat transfer enhancement levels comparable to higher mist loading fraction amounts in excess of 0.1.

Keywords: *Atomizing mist jet, heat transfer, two-phase cooling, hotspot cooling*

1. INTRODUCTION

Impinging air jets have long been known to achieve superior heat transfer coefficients, with the variation in their local characteristics also lending itself to application in hot spot cooling. Their ability to achieve effective cooling rates has led to the implementation of jet cooling in many situations including applications such as electronics cooling or grinding. Although air jet impingement cooling is effective, the addition of suspended liquid droplets yields further improvement in cooling performance, as seen in previous work within the research group [1].

The dispersal of liquid droplets into a gaseous flow can be characterised as either spray cooling or mist jet cooling. In spray cooling, the energy to atomize the water is provided by the pressure drop that exists in the liquid supply across a narrow nozzle exit, whereas in mist jet cooling a high velocity co-flowing air stream atomizes the water, typically resulting in smaller water droplets than a spray, as observed by Lee et al. [2]; this process is known as shear driven atomization.

The introduction of a fine water mist into an air jet leads to an increase in heat transfer rates, as observed by [2] for water droplet diameters of 30-80 μm. Convective heat transfer coefficients were found to increase up to 10 times compared to a single phase air jet through evaporation of a thin liquid film 50-100 μm thick. Previous work in this area can be grouped into water/air mist, such as the study conducted by Sozbir et al. [3], and mist/steam, as reported by Li et al. [4]; generally these studies have focussed on high wall temperatures. Lyons et al. [1] presented results for an atomizing mist jet at similar wall temperatures to this study. The authors found that even small amounts of water in a mist jet led to significant increases in the convective heat transfer coefficient. It was also seen that an increase in water mass flow rate did not necessarily lead to an increase in the stagnation zone heat transfer. However, the higher water flow rate maintained higher levels of the convective heat transfer coefficient for greater radial distances.

This paper presents research on the heat transfer characteristics of an impinging atomizing air-water mist jet. Time averaged heat transfer results have been obtained by a differential thermopile sensor. This paper seeks to understand the linkage between fractional mist loading and the heat transfer characteristics of the mist

jet. This study follows on from the work of Lyons et al. [1], but uses a different atomizing nozzle with a simpler geometry; results are presented also for a broader range of Reynolds numbers and mist loading ratios.
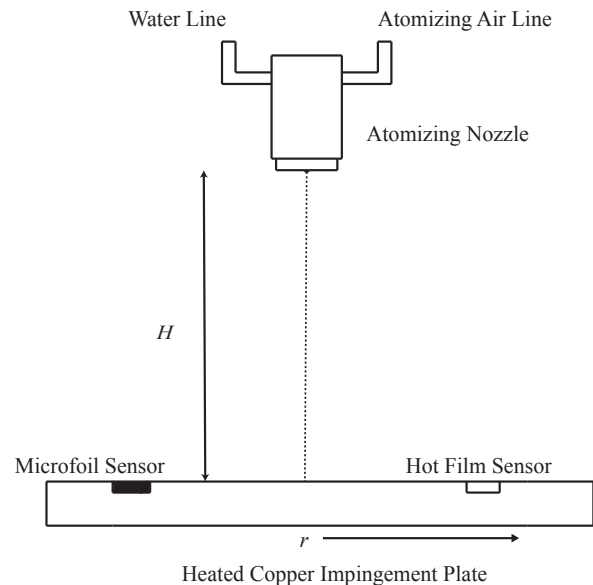
2. EXPERIMENT

Figure 1: Schematic of test apparatus

An experimental rig has been built to investigate the heat transfer characteristics of an impinging mist jet. The test surface is an instrumented isothermally heated copper plate. The local heat flux from the surface to the jet flow is measured using a thermopile RdF micro-foil heat flux sensor mounted flush to the copper plate. The thermopile sensor is used to obtain time averaged heat transfer coefficients. The micro-foil sensor consists of 3 thin layers of kapton with T-type thermopiles on either side of the central layer. The thermal conductivity and thickness of the kapton layer is known,
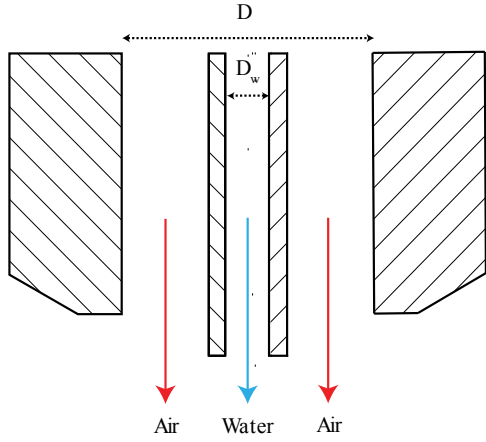
Figure 2: Nozzle exit (not to scale)

therefore the heat flux through the sensor can be calculated using the temperature difference determined from the thermopile readings. The output signal of the thermopile sensor (RdF 27036-1) is amplified by a factor of 1000. The thermopile sensor also contains a thermocouple, which is used to measure the wall temperature. Another thermocouple is placed in the air inlet line to measure the jet temperature. Figure 1 presents a schematic of the experimental set-up. The hot film sensor shown is used to measure heat transfer fluctuations, though these do not form part of the present investigation.

Figure 2 shows a detailed cross sectional view of the nozzle exit for illustration purposes. The mist jet consists of a central water jet, which is atomized by a co-flowing concentric annular air jet. D is the diameter of the annular jet, or the outer jet diameter, and D_w is the diameter of the central water jet. In the atomization process the water droplets are injected into the air flow in the initial mixing region of the annular jet and are entrained into the annular air flow. The air flow provides strong shear forces which act upon the water flow. These shear forces provide the energy necessary to atomize the water jet by air to water momentum transfer.

Heat transfer coefficients associated with the mist jet are calculated using the expression:

$$h(x) = \frac{q"_{conv}(x)}{T_{wall}(x) - T_{jet}} \qquad (1)$$

where $q"_{qonv}$ is the convective heat flux, T_{wall} is the wall temperature as measured by the thermopile thermocouple and T_{jet} is the jet temperature as measured by the thermocouple in the air jet.

The nozzle used is a Spraying Systems B1/4 VMAU-316 SS nozzle. In all results, the radial displacement, r, and the nozzle to plate spacing, H, are both normalized by the outer nozzle diameter, D, which is 1.7251 mm. The Reynolds number is based on the velocity of the annular air jet, and the characteristic length for the Reynolds number is the hydraulic diameter, D_h, of the atomizing annular air nozzle, which is 0.44 mm. This choice takes into account the flow conditions at the nozzle exit and was used in previous work [1] and in the work of Ichimiya [5]. The Reynolds number is given by:
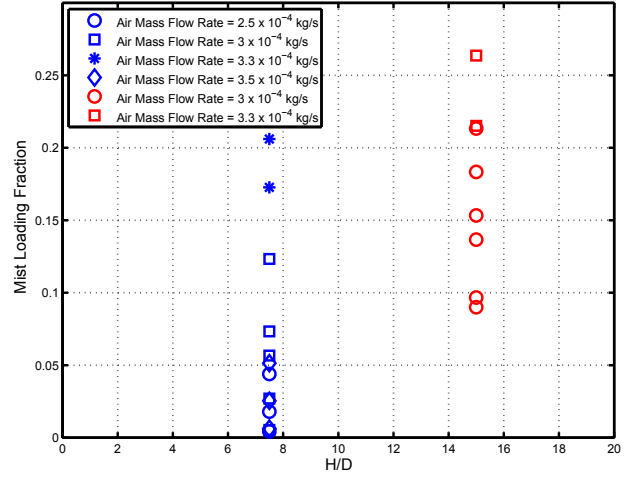
(a)
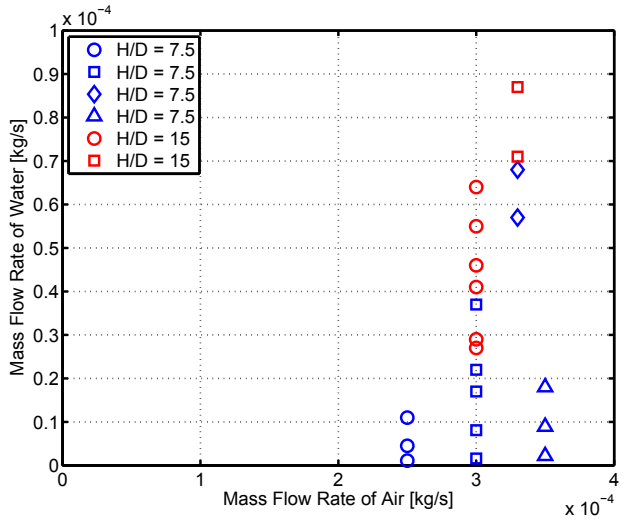
(b)

Figure 3: (a) Water and air mass flow rates for two H/D values and (b) mist loading fractions for two H/D values used in testing - H/D = 7.5 and 15.

$$Re = \frac{uD_h}{\nu} \qquad (2)$$

where u is the air jet velocity and ν is the kinematic viscosity of air.

The mist loading fraction, f, is defined as:

$$f = \frac{\dot{m}_w}{\dot{m}_a} \qquad (3)$$

where $\dot{m}_w$ is the mass flow rate of water and $\dot{m}_a$ is the mass flow rate of air. This definition is the same as that used by Kumari et al. [6] and also used by Su et al. [7] who referred to the mist loading as the mass flow ratio. This study examines the effect of mist loading on the local heat transfer coefficient. Figure 3 (a) shows the combination of water and air mass flow rates which are used in equation 3 to calculate the mist loading fraction. The different mist loading fractions examined in this study are presented in figure 3 (b) for both nozzle to surface distances considered. An adjustable

Table 1: Summary of Mist Loading Fractions

Reynolds Number	6,900	8,900		10,200		11,100
H/D	7.5	7.5	15	7.5	15	7.5
Mist Loading Fraction	0.004	0.005	0.092	0.17	0.228	0.006
	0.018	0.026	0.098	0.204	0.26	0.023
	0.041	0.053	0.137			0.047
		0.072	0.153			
		0.118	0.183			
			0.21			

constant pressure head system was used to supply water to the nozzle, while the air flow is regulated using a flow control valve connected to a buffer vessel fed off the building compressed air grid. The air flow was measured using an Alicat Scientific M-500SLPM-D air flow meter, which has an accuracy of $\pm 0.8\%$. The water flow rate was measured by collecting the water from the mist jet over a measured period of time and determining the mass of water collected using a digital scales; from this the mass flow rate could be determined. The maximum uncertainty in the water flow rate measurements was 18%.

The mist loading fractions in this study range from 0.004 to 0.26. It was found that if the air mass flow rate was increased but the water pressure head was kept constant the mist loading fraction would also increase. As a constant water pressure head should have resulted in a constant water mass flow rate, and therefore a decrease in the mist loading fraction. The observed increase in mist loading suggests that the increased subpressure caused by the air jet at the nozzle exit draws in over-proportionally more water from the constant water pressure head supply. To place the current mist loading fractions in context, the mist loading fractions used by Babic et al. [8] in their study ranged from 0.015 to 0.042; Hernández-Bocanegra et al. [9] used mist loading fractions ranging between 0.008 and 0.31, though the 0.31 was an outlying parameter, and the majority of the loading fractions were less than 0.1. The study by Kumari et al. [6] used mist loading fractions of 0.01 and 0.10, although that work dealt with a mist flowing through a finned heat sink rather than an impinging mist jet. Thus, the current study encompasses a broader range of mist loadings than commonly considered.

Table 1 provides a summary of the different mist loadings for the two H/D values and four air Reynolds numbers examined in this study.

3. RESULTS AND DISCUSSION

In this section, the local heat transfer profiles obtained for a number of mist loading fractions and at four air Reynolds numbers and two H/D values are presented. Local heat transfer profiles from earlier work by the authors [1] are also included.

3.1. Convective heat transfer profiles

Previous work [1] has shown an improvement in cooling performance for a mist jet over the performance of an air only jet. This has been observed in the current study, with enhancement levels
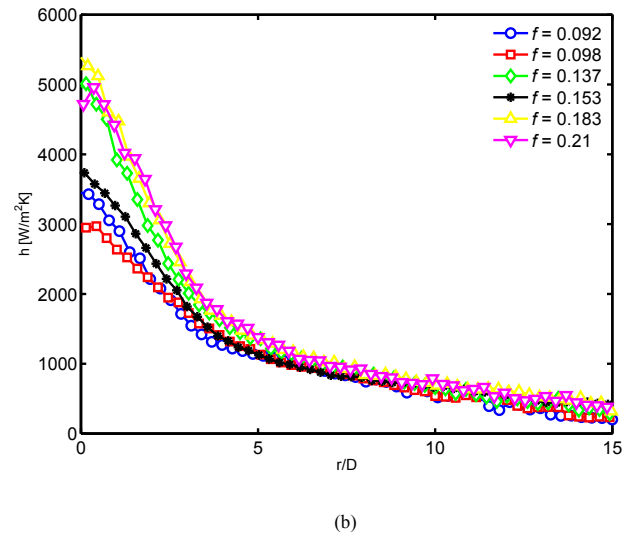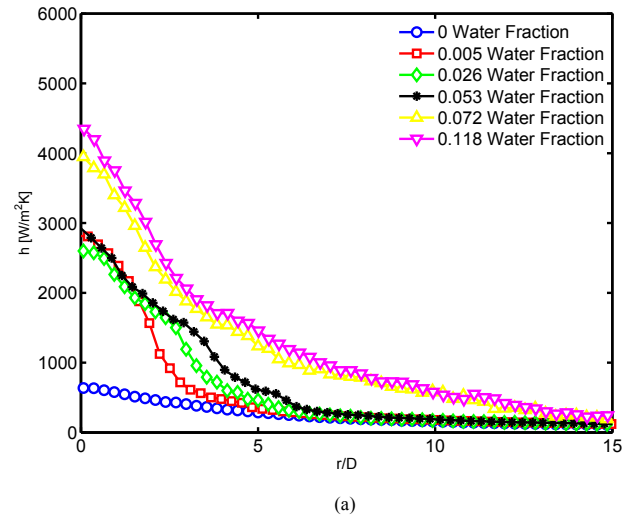

(a)

(b)

Figure 4: Mist jet heat transfer profiles for varying water loading fractions at a Reynolds number of 8,900 and (a) $H/D = 7.5$ and (b) $H/D = 15$.

of the order of 500% being observed in the stagnation zone. Figures 4, 5 and 6, for varying Reynolds number and nozzle to plate distances, all show this to be the case. As the radial distance increases, the mist jet profiles collapse to the same level as the air only profile; however with higher mist loading fractions this
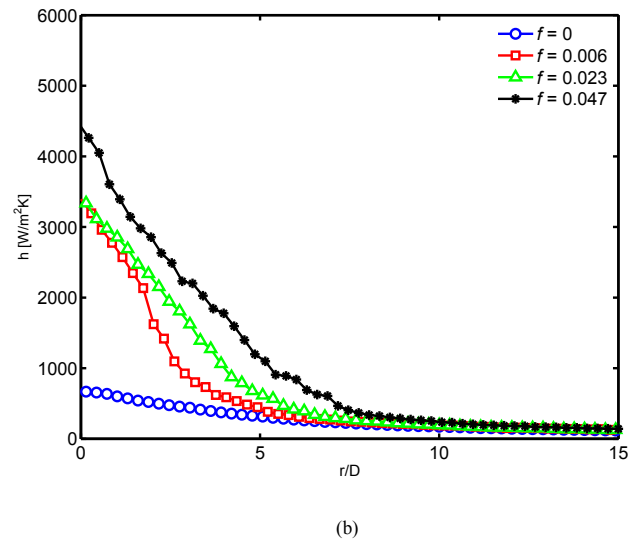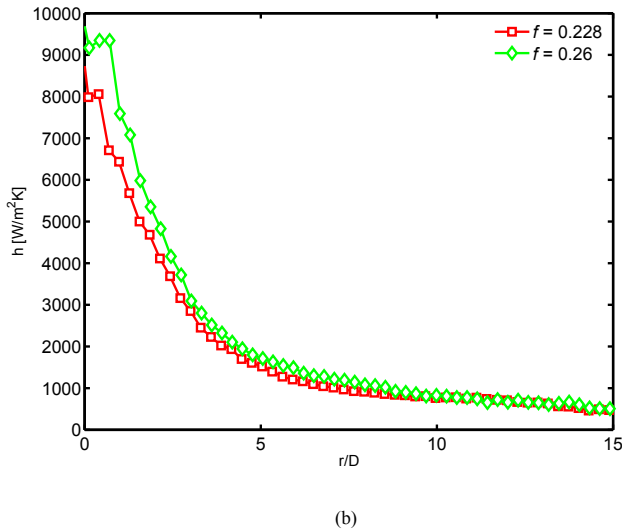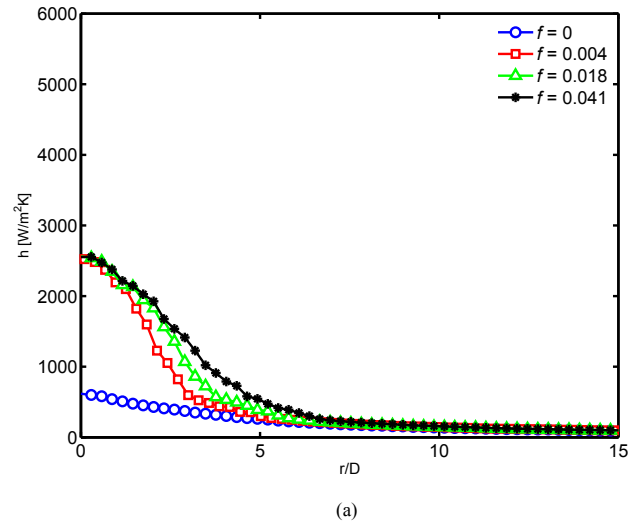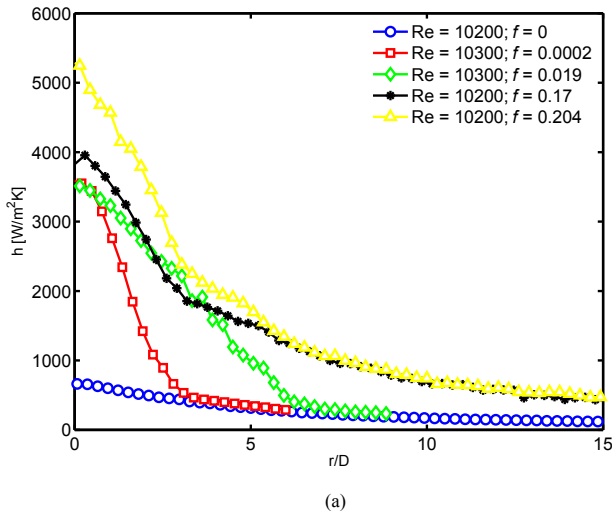
(a)

(b)

Figure 5: Mist jet heat transfer profiles for varying mist loading fractions and (a) $H/D = 7.5$ and Reynolds numbers of 10,200 and 10,300 and (b) $H/D = 15$ and Reynolds number equals 10,200

(a)

(b)

Figure 6: Mist jet heat transfer profiles for varying mist loading fractions at $H/D = 7.5$ and (a) a Reynolds number of 6,900 and (b) a Reynolds number of 11,100

collapse happens at greater radial distances.

Figures 4, 5 and 6 all show the typical bell shaped curve associated with the heat transfer coefficient for an impinging jet at high H/D, though the heat transfer rate appears to undergo a sharper drop off than is typical for an air only flow. This was also observed by Lyons et al. [1]. Due to the relatively low surface temperature, the mist jet causes pooling of water at a radial distance greater than approximately 10 diameters. This is particularly the case for higher water mass fractions. This pooling has a negative impact on the effectiveness of the jet. The greater the radial distance from the stagnation zone, the lower the energy of the air flow, and as such the air jet is no longer able to move the water along the surface which leads to this pooling. The variability in heat transfer distributions observed at radial distances greater than 10 diameters can most likely be attributed to pooling and to the disturbance of the pools by the air jet; these variations are particularly noticeable in figure 4 (b) between r/D values of 10 and 15.

In figure 4 (a) it can be seen that a small increase in the water

fraction - from 0.054 to 0.072 - leads to a dramatic increase in the stagnation heat transfer coefficient. This increase in mist loading led to a significantly larger amount of water gathering on the surface; for the 0.054 fraction there was very little visible water on the surface in the stagnation zone, whereas in the case of the 0.072 fraction there was a noticeable layer of water that remained on the surface, even in the stagnation zone. This layer of water could be increasing the stagnation heat transfer due to there being a thicker liquid film undergoing evaporation in the higher fraction profiles. Further study at intermediate loading fractions may elucidate this phenomenon. At lower mist loading fractions, increasing this parameter does not necessarily give rise to an increase in the stagnation heat transfer coefficient. However it has been observed that increasing the mist fraction increases the radial spread of the heat transfer enhancement; this can be seen most clearly in figure 4 (a), and in figure 6 (a) and (b). Using shadowgraph data, Lyons et al. [1] attributed this to the fact that a greater number of larger droplets spread further radially for higher water fractions.
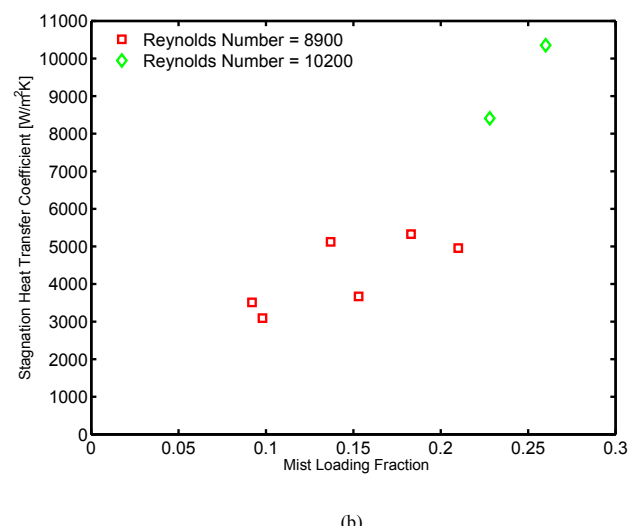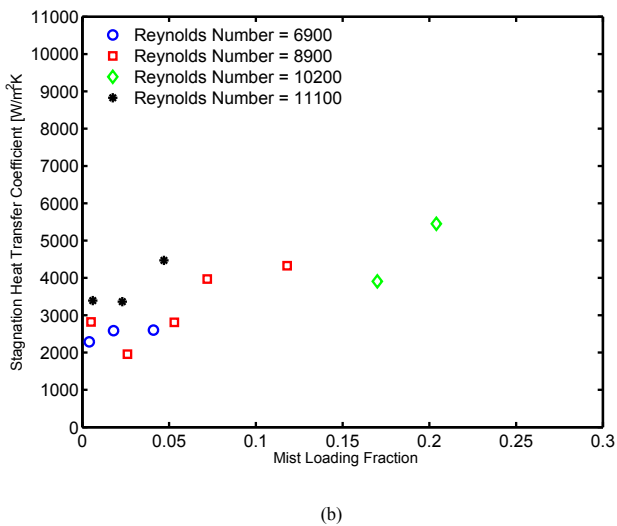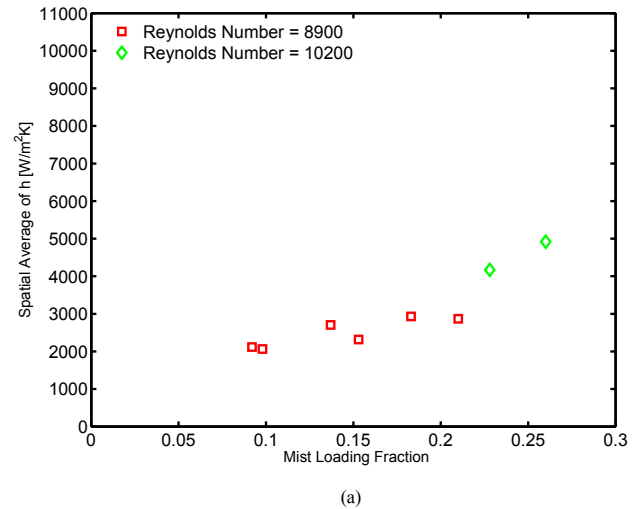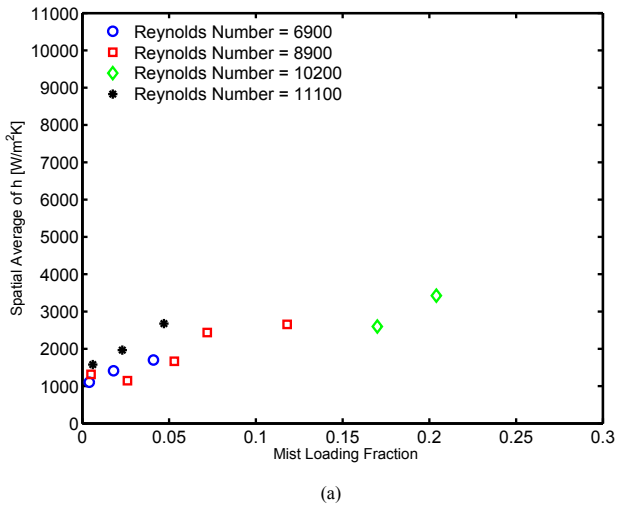
(a)

(b)

Figure 7: For $H/D = 7.5$, (a) spatial averages of heat transfer coefficient and (b) stagnation point heat transfer coefficient

(a)

(b)

Figure 8: For $H/D = 15$, (a) spatial averages of heat transfer coefficient, (b) stagnation point heat transfer coefficients

For the higher water mass fractions, particularly 0.072 and 0.118 in figure 4 (a), this radial spreading of enhancement is observed; however the two profiles are very similar. This may be attributed to increased pooling at higher water fractions as discussed above.

Overall, there is significant variability in the stagnation heat transfer coefficient with changes in the water fraction. In figure 4 (b) the 0.137 water fraction gives rise to a higher stagnation heat transfer rate than the 0.153 fraction, and it is comparable to the heat transfer for the two highest fractions. This may indicate that there is an optimum water fraction for maximising the heat transfer, above which any extra water may be superfluous. Further work at very refined water fractions is required to confirm this.

By comparing figures 4, 5 and 6, it can be seen that increasing the air Reynolds number leads to an increase in the stagnation zone heat transfer., though as the radial distance increases the dependence on Reynolds number appears to diminish and disappear.

Included in figure 5 (a) are two heat transfer profiles previously reported by Lyons et al. [1] for a near identical Reynolds number. The nozzle geometry used in those tests is different from that of the current study. Despite this, the profiles fit the general trend

reported here. The mist loading fractions for the two profiles are considerably lower than those from the current study in figure 5; as such the radial spreading of the enhancement is less for the lower mist fractions, and the stagnation point heat transfer coefficients are slightly lower. Despite the much lower mist loading fraction, significant heat transfer enhancement can be seen; stagnation zone heat transfer in these profiles is similar in magnitude to that of the current study. One of the main conclusions of [1] was that even a small amount of mist resulted in a large enhancement in heat transfer. This finding has been confirmed by the current study. Lyons et al. [1] suggested the frequency of the atomization of the water and the droplet intensity were contributing factors in this result, though further work at very low mist loading fractions is important to fully understand the reason behind this.

In the work of Oliphant et al. [10] it was also reported that high heat transfer coefficients were obtained using a spray with relatively low liquid mass flow rates. A further finding was that the average heat transfer coefficient for the spray increased with decreasing liquid mass flow rate, a finding reported in some cases

in the current study. Although the work of [10] relates to a spray rather than a mist jet, the results serve to validate the current findings.

3.2. Spatial averages of the heat transfer coefficient and stagnation point heat transfer coefficients

Figures 7 (a) and (b) are plots of the spatial averages of the heat transfer coefficients over a radial zone extending up to 5 diameters from the stagnation point, and the stagnation point heat transfer coefficients respectively at $H/D = 7.5$. Figures 8 (a) and (b) show the same plots for $H/D = 15$.. As expected, the spatial averages are lower than the stagnation point heat transfer for the same water mass fraction and Reynolds number. However, as the stagnation point heat transfer relates to a very small area, the spatial average provides a better picture of the overall heat transfer effectiveness of the mist jet. As the heat transfer profiles show that with increasing water fraction the heat transfer enhancement of the mist spreads radially, the spatial average becomes an important indicator of the heat transfer performance of the mist jet.

Figure 7 shows that the stagnation heat transfer and the spatial average of the heat transfer do not follow the same trends for the same water fractions and Reynolds numbers. Figure 7 (b) shows that increasing the water fraction does not necessarily lead to a noticeable increase in the stagnation heat transfer; in some cases it actually tends to decrease the stagnation heat transfer. However, increasing the water fraction leads to an increase in the spatial average of the heat transfer coefficients for each Reynolds number presented in figure 7 (a). This indicates the importance of the radial enhancement as discussed above. The effect of air Reynolds number can also be seen in figure 7. As the Reynolds number increases so too does the spatial average; again the trends in the stagnation heat transfer differ from those of the spatial averages.

This trend is less evident for the spatial averages of the heat transfer coefficient and the stagnation heat transfer coefficient for a H/D value of 15, which is shown in figure 8. Here, the two plots follow very similar patterns, with outlying values in the stagnation heat transfer coefficients also visible in the spatial average plot. Further work with more water fractions at this H/D is needed to determine if this is due to the plate to nozzle spacing or to some other effect.

4. CONCLUSION

This study has been undertaken to characterise the heat transfer performance of an atomizing water-air mist jet. The addition of a water mist to the air jet was found to enhance the local heat transfer coefficient in the stagnation zone and led to radial spreading of the heat transfer enhancement. The effect of Reynolds number and nozzle to plate spacing was also examined. The results of this study were compared with results from previous work by the authors [1] and found to fit the same general trend. Thus, very small mist loading fractions were seen to lead to a significant cooling performance enhancement; this enhancement was of the same order as that of much higher mist loading fractions. Further study at very low mist loading fractions is important to fully understand the process by which this happens.

The effects of varying mist loading was examined. It was found that increasing the mist loading fraction did not necessarily lead to a further enhancement of the stagnation heat transfer coefficient. However, with increasing mist loading fraction, the radial spread of the heat transfer enhancement was seen to increase. The spatial averages of the heat transfer coefficient confirmed this. As the stagnation point heat transfer refers to a very small area, the spatial averages provide a more complete picture of the cooling performance of the mist jet, although hot spot cooling is dependent on the stagnation zone heat transfer.

At high mist loading fractions, there was little difference between the heat transfer profiles for different mist loading fractions at the same Reynolds number and nozzle to plate spacing. This suggests there may be an optimum mist loading fraction above which any further addition of water is superfluous. Further work with finer increases in mist loading fraction may confirm this.

Measurement of the fluctuating component of the heat transfer coefficient is expected to provide a more complete analysis of the heat transfer characteristics of the water-air mist jet. Analysis using flow visualisations, such as PIV and shadowgraphy, will provide important information regarding the flow field, and how the structure of the mist jet affects the heat transfer performance.

5. ACKNOWLEDGEMENTS

REFERENCES

1. O. F. Lyons, C. Quinn, T. Persoons, and D. B. Murray, Heat transfer and flow in an atomizing mist jet: a combined hot film and shadowgraph imaging approach, in *Journal of Physics: Conference Series*, vol. 395, p. 012173, IOP Publishing, 2012.

2. S. Lee, Z. Yang, and Y. Hsyua, Cooling of a heated surface by mist flow, *Journal of Heat Transfer*, vol. 116, pp. 167–172, 1994.

3. N. Sozbir, Y. Chang, and S. Yao, Heat transfer of impacting water mist on high temperature metal surfaces, *Journal of Heat Transfer*, vol. 125, pp. 70–74, 2003.

4. X. Li, J. Gaddis, and T. Wang, Mist/steam heat transfer in confined slot jet impingement, *Transactions of the ASME-T-Journal of Turbomachinery*, vol. 123, pp. 161–167, 2001.

5. K. Ichimiya, Heat transfer characteristics of an annular turbulent impinging jet with a confined wall measured by thermosensitive liquid crystal, *Heat and Mass Transfer*, vol. 39, pp. 545–551, 2003.

6. N. Kumari, V. Bahadur, M. Hodes, T. Salamon, P. Kolodner, A. Lyons, and S. V. Garimella, Analysis of evaporating mist flow for enhanced convective heat transfer, *International Journal of Heat and Mass Transfer*, vol. 53, pp. 3346–3356, 2010.

7. L. M. Su, S. Chang, C. Yeh, and Y. Hsu, Heat transfer of impinging air and liquid nitrogen mist jet onto superheated flat surface, *International Journal of Heat and Mass Transfer*, vol. 46, pp. 4845–4862, 2003.

8. D. Babic, D. Murray, and A. Torrance, Mist jet cooling of grinding processes, *International Journal of Machine Tools and Manufacture*, vol. 45, pp. 1171–1177, 2005.

9. C. Hernández B, J. Minchaca M, A. Castillejos E, F. Acosta G, X. Zhou, and B. G. Thomas, Measurement of heat flux in dense air-mist cooling: Part ii. the influence of mist characteristics on steady-state heat transfer, *Experimental Thermal and Fluid Science*, vol. 44, pp. 161–173, 2012.

10. K. Oliphant, B. Webb, and M. McQuay, An experimental comparison of liquid jet array and spray impingement cooling in the non-boiling regime, *Experimental Thermal and Fluid Science*, vol. 18, pp. 1–10, 1998.